Electronic Supplementary Information for

Germanium-Regulated Adsorption Site Preference on Ruthenium Electrocatalyst for Efficient Hydrogen Evolution

Meihong Fan,[a,b] Bo Zhang,[c] Lina Wang,[a] Zhenyu Li,[a] Xiao Liang,[a] Xuan Ai[a] and Xiaoxin Zou*[a]

[a] *State Key Laboratory of Inorganic Synthesis and Preparative Chemistry, College of Chemistry, Jilin University, Changchun 130012, China*

[b] *State Key Laboratory of Superhard Materials, College of Physics, Jilin University, Changchun, 130012, China*

[c] *International Center of Future Science, Jilin University, Changchun, 130012 China*

* E-mail: xxzou@jlu.edu.cn

1. Theoretical Section

1.1. Computation Details.

All the calculations were performed by using the Perdew-Burke-Ernzerhof (PBE)[1] exchange-correlation functional within the generalized gradient approximation (GGA) in the framework of *Vienna ab initio simulation package* (VASP)[2-3] based on the density functional theory (DFT). For all the structural relaxations and electronic structure calculations, the cut off energy of plane-wave set[4] was 400 eV, while the convergence threshold was set as 0.02 eV/Å in force and 10^{-4} eV in energy. For the bulk calculations, the Brillouin zones were sampled by Monkhorst-Pack 11×11×7 and 5×5×5 k-point grid for Ru and RuGe, respectively. For the slab models, the appropriate Monkhorst-Pack *k*-point meshes 5×5×1 for Ru and 3×3×1 for RuGe were employed. A 5×5×1 Monkhorst-Pack grid was used for the DOS calculations of slab models.[5] During the surface calculations, the symmetrization was switched off and the dipolar correction was included. The DFT-D2 method[6] was used to correct the *van der Waals* interaction. The crystal orbital Hamiltonian population (COHP) was obtained by LOBSTER code.[7-10]

For the slab models, we constructed 2 × 2 supercells for Ru and RuGe by cleaving the bulk structure along the (001) direction, and both of them contain 4 metal atom layers. A vacuum layer of 15 Å between slabs was added to avoid inter-layer interactions, and the upper half of atom layers were relaxed while the remaining were kept frozen during the slab calculations.

1.2. Computations of Free-Energy for the Hydrogen Evolution Reaction.

The Gibbs free-energy (ΔG_{H*}) of the hydrogen adsorption for different sites was calculated by the formula: $\Delta G_{H*} = \Delta E_{H*} + \Delta ZPE - T\Delta S$. ΔE_{H*} is the adsorption energy, which is defined as $\Delta E_{H*} = E(\text{surface} + H) - E(\text{surface}) - 1/2\ E(H_2)$, where E(surface + H) and E(surface) are the energy of one hydrogen atom adsorbed on the surface and the bare surface, while $E(H_2)$ is the energy of a gas phase H_2 molecule. ΔZPE and ΔS are the zero point energy and entropy change.[11] ΔZPE can be calculated by using the equation ΔZPE = ZPE (H*) – 1/2ZPE (H_2), and $T\Delta S$ can be obtained from the equation $T\Delta S \approx -1/2\ TS(H_2)$. Since TS (H_2) is 0.41eV for H_2 at 298K and 1atm, the corresponding $T\Delta S \approx -0.205$ eV.

Table S1 The energy E (eV) and formation enthalpy ΔH (eV) per formula unit for various structures.

Formula	RuGe	$MgCl_2$	$RuCl_3$	Ru	Mg	Ge	Cl_2
Energy (eV)	−15.370	−10.779	−16.771	−9.204	−1.536	−4.480	−3.594
Formation enthalpy (eV)	**−1.326**	**−5.649**	**−2.176**				

The formation enthalpies per formula unit of RuGe, $MgCl_2$ and $RuCl_3$ were calculated by

$\Delta H_F(\mathrm{RuGe}) = [E(\mathrm{RuGe}) - E(\mathrm{Ru}) - E(\mathrm{Ge})]$.

$\Delta H_F(\mathrm{MgCl_2}) = [E(\mathrm{MgCl_2}) - E(\mathrm{Mg}) - E(\mathrm{Cl_2})]$.

$\Delta H_F(\mathrm{RuCl_3}) = [E(\mathrm{RuCl_3}) - E(\mathrm{Ru}) - 1.5E(\mathrm{Cl_2})]$.

The reaction enthalpies of route I and route II were calculated according to the reaction equations of

Route I: Ru + Ge = RuGe

Route II: $RuCl_3$ + Ge + 1.5Mg = RuGe + 1.5$MgCl_2$

Their reaction enthalpies were calculated according to the formula:

$$\Delta H_R = \Delta H_F(\mathrm{R}) - \Delta H_F(\mathrm{S}) \qquad (1)$$

$\Delta H_F(\mathrm{S})$ and $\Delta H_F(\mathrm{R})$ are formation enthalpies of the starting and resulting compounds, which are listed are listed in **Table S1**.

2. Experimental Section

2.1. Chemicals and Reagents.

Ruthenium(III) chloride ($RuCl_3$), molybdenum(V) chloride ($MoCl_5$, 99.6%), palladium chloride ($PdCl_2$, 99.9%), platinum tetrachloride ($PtCl_4$, 99.9%), ruthenium oxide (RuO_2, 99.9%), germanium powder (Ge, 99.9%), ruthenium powder (Ru, 99.9%) were purchased from Aladdin Chemistry Co., Ltd. Magnesium powder (Mg) was purchased from Shantou Xilong Chemical Factory. Isopropanol ($(CH_3)_2CHOH$) and Sulfuric acid (H_2SO_4) were purchased from Beijing Chemical Factory. Nafion® perfluorinated resin solution were purchased from Sigma-Aldrich. Highly purified water (> 18 MΩ cm resistivity) was obtained from a PALL PURELAB Plus system.

2.2 Materials Synthesis.

Synthesis of RuGe. $RuCl_3$ (51.9 mg, 0.25 mmol), Ge (7.0 mg, 0.25 mmol) and Mg (14.6 mg, 0.5 mmol) were transferred into a quartz tube, which was then sealed in a vacuum atmosphere (1.0 Pa). Next, the sealed quartz tube was heated at 800 °C for 4 h. The obtained product was treated in a 0.5 M H_2SO_4 solution to remove redundant Mg and by-product (*i.e.*, $MgCl_2$). Finally, the resulting sample was washed several times with deionized water and ethanol, and vacuum dried at 80 °C.

Synthesis of $MoGe_2$. $MoCl_5$ (68.3 mg, 0.25 mmol), Ge (36.3 mg, 0.5 mmol) and Mg (15.2 mg, 0.63 mmol) were transferred into a quartz tube, which was then sealed in a vacuum atmosphere (1.0 Pa). Next, the sealed quartz tube was heated at 800 °C for 4 h. The obtained product was treated in the same method as the RuGe.

Synthesis of PtGe. $PtCl_4$ (84.2 mg, 0.25 mmol), Ge (18.2 mg, 0.25 mmol) and Mg (14.6 mg, 0.5 mmol) were transferred into a quartz tube, which was then sealed in a vacuum atmosphere (1.0 Pa). Next, the sealed quartz tube was heated at 800 °C for 4 h. The obtained product was treated in the same method as the RuGe.

Synthesis of Pd_2Ge. $PdCl_2$ (44.3 mg, 0.25 mmol), Ge (18.2 mg, 0.25 mmol) and Mg (7.3 mg, 0.25 mmol) were transferred into a quartz tube, which was then sealed in a vacuum atmosphere (1.0 Pa). Next, the sealed quartz tube was heated at 700 °C for 4 h. The obtained product was treated in the same method as the RuGe.

Synthesis of Ru. $RuCl_3$ (51.9 mg, 0.25 mmol) and Mg (14.6 mg, 0.6 mmol) were transferred into a quartz tube, which was then sealed in a vacuum atmosphere (1.0 Pa). Next, the sealed quartz tube was heated at 700 °C for 4 h. The obtained product was treated in the same method as the RuGe.

Synthesis of Pt. $PtCl_4$ (84.2 mg, 0.25 mmol) and Mg (24.3 mg, 1.0 mmol) were transferred into a quartz tube, which was then sealed in a vacuum atmosphere (1.0 Pa). Next, the sealed quartz tube was heated at 500 °C for 4 h. The obtained product was treated in the same method as the RuGe.

2.3. Characterizations.

Powder X-ray diffraction (XRD) were collected using a Rigaku D/Max 2550 X-ray diffractometer with Cu Kα radiation (λ = 1.5418 Å). The scanning electron microscope (SEM) images were obtained with a JEOL JSM 7800F electron microscope. The transmission electron microscope (TEM) and high

resolution TEM (HRTEM) images were recorded on a Philips-FEI Tecnai G2STwin microscope equipped with a field emission gun operating at 200 kV. X-ray photoemission spectroscopy (XPS) studies were performed on a Thermo Fisher Scientific ESCALAB 250Xi with photoelectron spectroscopy system using a monochromatic Al Ka (1486.6 eV) X-ray source.

2.4. Electrochemical Measurements.

Electrochemical measurements were carried out using a CH Instrument (Model 660E) with a conventional three-electrode system: glassy carbon electrode (GCE) loaded with catalyst as the working electrode, saturated calomel electrode (SCE) as the reference electrode, and carbon rod as the counter electrode. The electrolyte was 0.5 M H_2SO_4 solution.

The calomel electrode calibration was performed according to the method used by our group previously,[14] and the calibrated value (E^{o}_{SCE}) was 0.267 V. Calibrations were performed using a reversible hydrogen electrode (RHE), which was made up of two Pt as working electrode and counter electrode, and SCE as reference electrode, respectively. H_2 is bubbled over the working electrode. Two Pt electrodes were cleaned and cycled in 0.5 M H_2SO_4 solution (about ± 2 V) prior to use. The electrolyte was saturated with hydrogen before use and hydrogen was bubbled over the working electrode during the test. The wide-ranged Linear sweep voltammetry (LSV) was measured in a cathode to determine possible zero-current potential. Then controlled potential chronoampermetric tests were performed to further determine the zero-current potential. It was necessary to stabilize for 300 s to reach the steady state value under each potential.

The working electrode was prepared by the following steps: (1) 4 mg of catalyst was uniformly dispersed in 200 μL of isopropanol and 200 μL of conductive polymer binder (0.3% Nafion solution); (2) 4 μL of this solution was dropped onto a GCE with a diameter of 3 mm, and then dried in the air; (3) 1 μL of 0.3% Nafion solution was dropped on top and dried. The loading mass was 0.56 mg cm^{-2}.

LSV measurements were performed with the scan rate of 1 mV/s and 85% *iR*- compensation. Chronopotentiometric measurements were studied at a current density of 10 mA cm^{-2} without *iR*-compensation. The obtained potentials were converted to the potentials *vs* reversible hydrogen electrode (RHE) according to the formula:

$$E_{vs.RHE} = E_{vs.SCE} + 0.267\ eV + 0.059\ pH \qquad (2)$$

The geometric current density j_{geo} (mA cm^{-2}) was normalized by the geometric area of working electrode according to the formula:

$$j_{goe} = \frac{i \times 1000}{S} \qquad (3)$$

where *i* (A) is the obtained current, and *S* is the geometric area of working electrode (0.071 cm^2).

The mass activity of ruthenium j_{Ru} (A g^{-1}) was obtained by normalizing the measured current with respect to the mass of ruthenium according to the following equations:

$$j_{Ru} = \frac{i \times 1000}{m \times WRu} \qquad (4)$$

where i (A) is the obtained current, m is catalyst mass loading (4×10^{-5} g), and W_{Ru} is weight percent of ruthenium (wt%) in the catalyst.

The specific activity j_{ECSA} (mA cm^{-2}) was normalized by the electrochemical active surface area (ECSA) according to the formula:

$$j_{ECSA} = \frac{i \times 1000}{ECSA} \qquad (5)$$

where i (A) is the obtained current, and ECSA is the corresponding electrochemical surface area of catalyst.

The ECSA of catalyst was estimated by CO stripping experiments.[15] 99.99% pure CO was purged to the cells filled with 0.5 M H_2SO_4 electrolyte for 30 min, while the working electrode was held at 0.02 V *vs.* SCE. Before the measurements, N_2 was then purged to the system for 30 min to remove non-adsorbed CO. The CO stripping was performed in the potential range of -0.2~1.0 V at a scan rate of 0.5 V s^{-1} (**Fig. 3b**). Assuming that the Coulombic charge required for the oxidation of the CO monolayer was 0.42 mC cm^{-2}, and the ECSA was calculated according to the formula:

$$ECSA = \frac{Q_{CO}}{m \times 0.42\ (mC\ cm-2)} = \frac{S_{CO}/V}{m \times 0.42\ (mC\ cm-2)} \qquad (6)$$

Where Q_{CO} is the CO stripping charge, V is scan rate, and m is catalyst mass loading (4×10^{-5} g).

2.5. TOF calculation.

The turnover frequency (TOF, H_2 s^{-1}) can be estimated by using the following equation:

$$\text{TOF} = \frac{i}{2nF} \qquad (7)$$

where i is the current during the LSV measurement; the factor, 2, is the number of electron involved in HER reaction; F is the Faraday constant (96485 C mol^{-1}); n is the number of active sites on corresponding electrode.

It is difficult to accurately estimate the number of active sites (n) in heterogeneous catalysis. There are usually two methods: (i) only quantifying the number of surface active sites on catalyst (n_1) to give a upper limit of TOF (TOF_1);[15] (ii) considering all metal atoms loaded on the electrode as active sites (n_2) to give a lower limit of TOF (TOF_2).[16] The calculated TOF_1 and TOF_2 values are shown in **Table S2**.

n_1 calculation. The CO stripping method was used for quantifying the number of surface active sites on catalysts.[17,18] In this method, n_1 (mol) was calculated on basis of the CO stripping charge (Q_{CO}) with the following equation:

$$n_1 = \frac{Q_{CO}}{2F} \qquad (8)$$

where F is the Faraday constant (96485 C mol^{-1}), and Q_{CO} is the CO stripping charge.

n_2 calculation. n_2 (mol) was the number of whole metal loading in the catalyst.

$$n_2 = \frac{m}{M} \qquad (9)$$

where m is catalyst mass loading (4×10^{-5} g), and M is the relative molecular mass of catalyst.

Table S2. Comparison of Q_{CO}, the number of active sites and TOF values (at the overpotential of 30 mV) of our synthesized RuGe, Ru and Pt catalysts.

Catalysts	Q_{CO} (mC)	Number of active sites (mol), n_1	TOF_1 at the overpotential of 30 mV (H_2 s^{-1})	Number of active sites (mol), n_2	TOF_2 at the overpotential of 30 mV (H_2 s^{-1})
RuGe	0.06	3.1×10^{-10}	5.2	2.3×10^{-7}	0.007
Ru	1.13	5.8×10^{-9}	0.1	4.0×10^{-7}	0.001
Pt	0.23	1.2×10^{-9}	5.4	2.1×10^{-7}	0.03

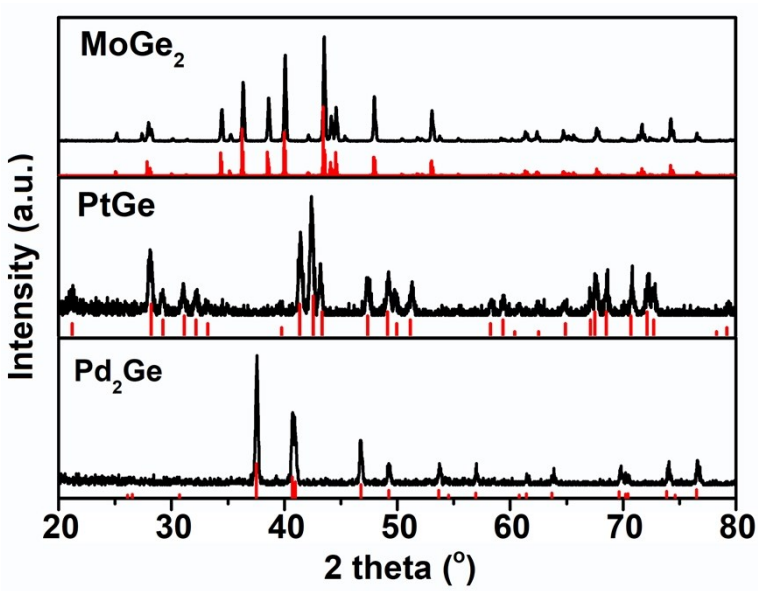

Fig. S1 The XRD patterns of $MoGe_2$, PtGe, and Pd_2Ge. For comparison, their standard XRD cards are included.

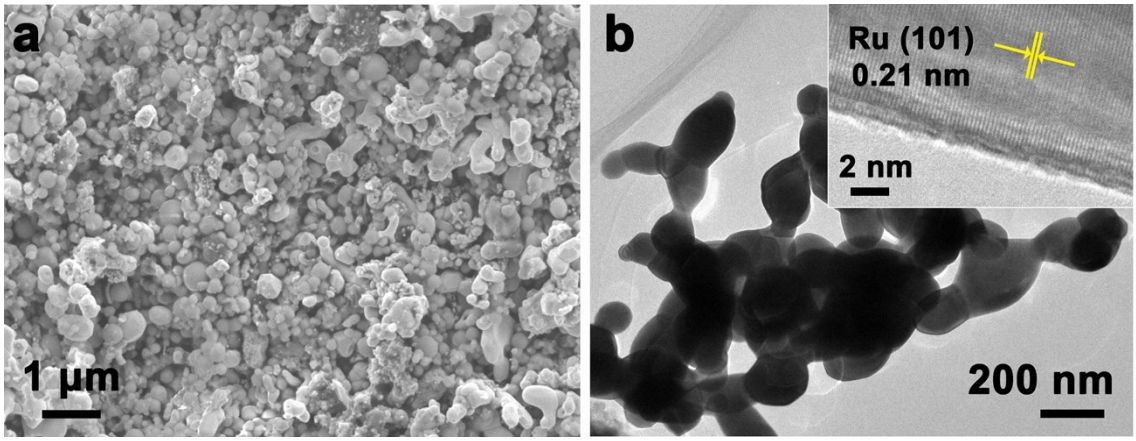

Fig. S2 (a) SEM, (b) TEM, and (b, inset) high-resolution TEM images of Ru. The sample is composed of particles of 100-500 nm size.

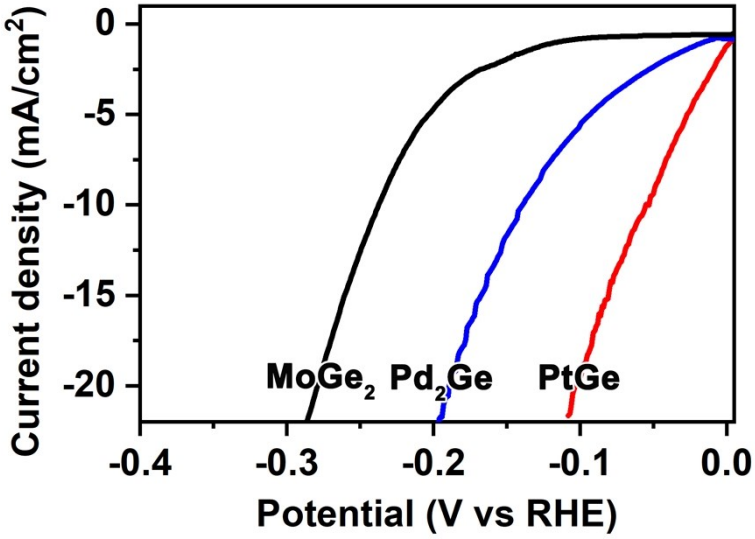

Fig. S3 Steady-state current density as a function of applied voltage during HER over $MoGe_2$, Pd_2Ge and PtGe in 0.5 M H_2SO_4 solution. The required overpotentials at a current density of 10 mA/cm^2 are 236 mV, 140 mV, and 54 mV, respectively.

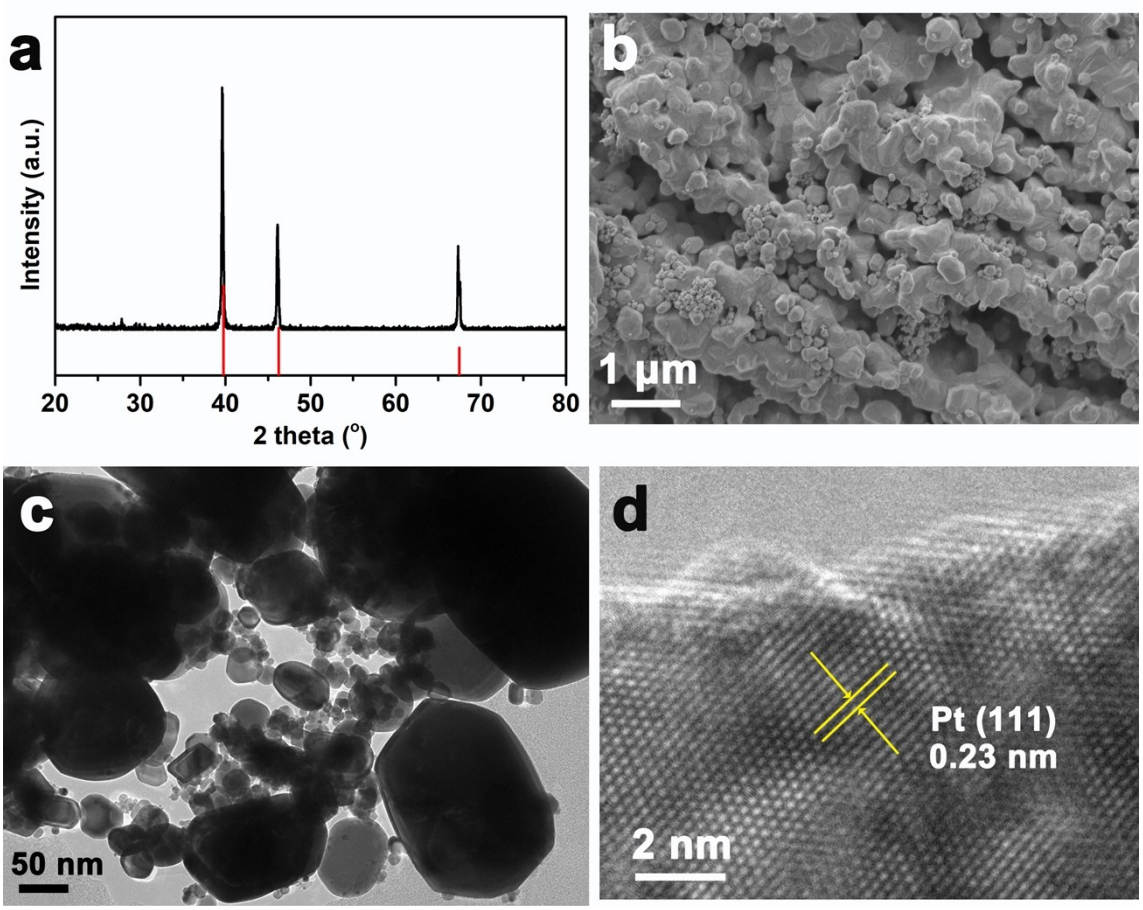

Fig. S4 (a) XRD, (b) SEM, (c) TEM, and (d) high-resolution TEM images of Pt. The particle size distribution is uneven ranging from 10 nm to 1 μm.

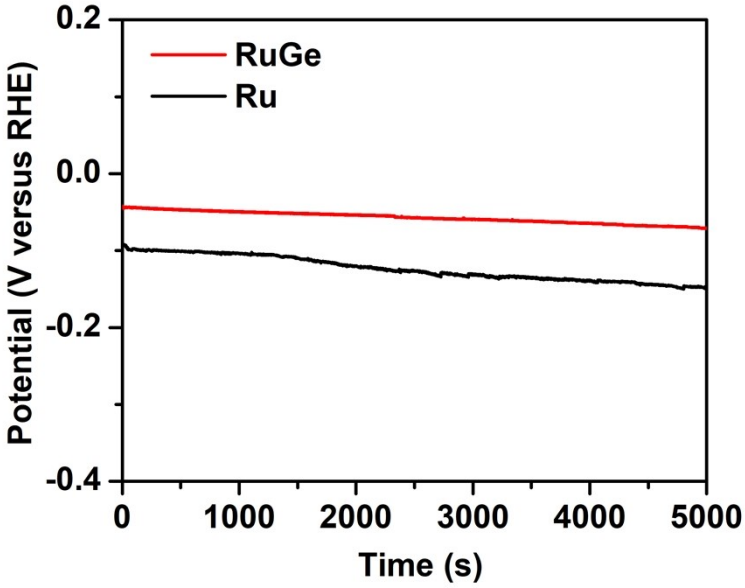

Fig. S5 Chronopotentiometric curves (V-t) with RuGe and Ru as catalysts at a current density of 10 mA cm^{-2} in 0.5 M H_2SO_4 solution.

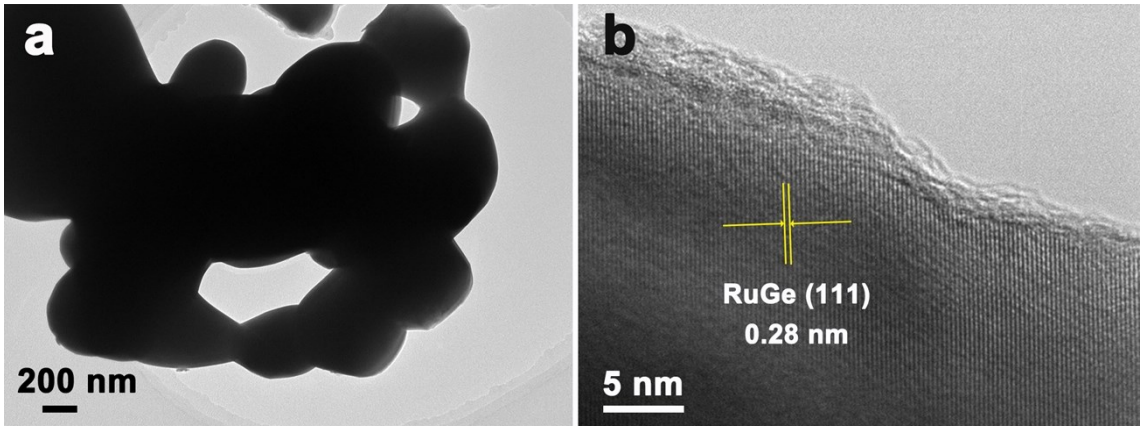

Fig. S6 (a) TEM and (b) HRTEM images of RuGe after electrocatalysis for HER in 0.5 M H_2SO_4 solution.

Table S3 Summary of some recently reported, representative Ru-based electrocatalysts for HER. Note that the calculated TOF_1 and TOF_2 values are the upper limit and lower limit of TOF, and their computation methods are shown in **part 2.5** and **Table S2**.

Catalysts	Mass loading (mg cm^{-2})	η at 10 mA cm^{-2} (mV)	j_{Ru} (A g^{-1})	TOF (s^{-1})	References
RuGe particles	**0.56**	**43**	**325.7 (100 mV)**	TOF_1=**5.2 (30 mV)** TOF_2=**0.007 (30 mV)**	**This work**
Ru particles	**0.56**	**98**	**18.9 (100 mV)**	TOF_1=**0.1 (30 mV)** TOF_2=**0.001 (30 mV)**	
RuB_2 particles	0.571	52	106.3 (100 mV)	–	[19]
Ru/RuS_2 nanosheets	0.849	45	<192.5 (110 mV)	0.71 (100 mV)	[20]
h-$RuSe_2$	0.3	34	341.9 (110 mV)	0.34 (30 mV)	[16]
$Cu_{53}Ru_{47}$ alloy	0.306	15	199.6 (50 mV)	1.14 (100 mV)	[21]
$RuTe_2$ nanorods	0.204	33	432 (60 mV)	–	[22]
PtPdRuTe	0.285	39	145.6 (46 mV)	0.94	[23]
RuNi@ carbon dots	0.418	58	1680 (13 mV)	5.03 (100 mV)	[24]
Ru single atoms@PN nanotubes	1	24	6060.6 (41 mV)	1.67 (25 mV); 4.29 (50 mV)	[25]
Ru@C_2N	0.285	22	366.8 (50 mV)	1.95 (50 mV)	[26]
Ru_2B_3@B, N-doped carbon	0.5	41	3030.3 (41 mV)	7	[27]
RuP_2@N, P-doped carbon	1	38	42.9 (38 mV)	–	[28]
Ru single atom @$Ti_3C_2T_x$	1	76	833 (76 mV)	0.52 (100 mV)	[29]
Ru particles @carbon	0.6	23	~100 (30 mV)	~0.2 (40 mV)	[30]
N-doped RuP@NPC	0.4	20.5	2500 (58.9 mV)	1.56 (30 mV)	[31]

Supplementary References

1. J. P. Perdew, K. Burke and M. Ernzerhof, *Phys. Rev. Lett.*, 1996, **77**, 3865.

2. G. Kresse and J. Furthmüller, *Comput. Mater. Sci.*, 1996, **6**, 15.

3. G. Kresse and J. Furthmüller, *Phys. Rev. B*, 1996, **54**, 11169.

4. P. E. Blöchl, *Phys. Rev. B*, 1994, **50**, 17953.

5. H. J. Monkhorst and J. D. Pack, *Phys. Rev. B*, 1976, **13**, 5188.

6. S. J. Grimme, *Comp. Chem.*, 2006, **27**, 1787.

7. R. Dronskowski and P. E. Blöchl, *J. Phys. Chem.*, 1993, **97**, 8617.

8. V. L. Deringer, A. L. Tchougreeff and R. Dronskowski, *J. Phys. Chem. A*, 2011, **115**, 5461.

9. S. Maintz, V. L. Deringer, A. L. Tchougreeff and R. Dronskowski, *J. Comput. Chem.*, 2013, **34**, 2557.

10. S. Maintz, V. L. Deringer, A. L. Tchougreeff and R. Dronskowski, *J. Comput. Chem.*, 2016, **37**, 1030.

11. J. K. Nørskov, T. Bligaard, A. Logadottir, J. R. Kitchin, J. Chen, S. Pandelov and U. Stimming, *J. Electrochem. Soc.*, 2005, **152**, 23.

12. M. S. Burke, M. G. Kast, L. Trotochaud, A. M. Smith and S. W. Boettcher, *J. Am. Chem. Soc.*, 2015, **137**, 3638.

13. C. C. L. McCrory, S. Jung, I. M. Ferrer, S. M. Chatman, J. C. Peters and T. F. Jaramillo, *J. Am. Chem. Soc.*, 2015, **137**, 4347.

14. Q. Li, X. Zou, X. Ai, H. Chen, L. Sun and X. Zou, *Adv. Energy Mater.*, 2019, **9**, 1803369.

15. G. Liu, W. Zhou, B. Chen, Q. Zhang, X. Cui, B. Li, Z. Lai, Y. Chen, Z. Zhang, L. Gu and H. Zhang, *Nano Energy*, 2019, **66**, 104173.

16. Y. Zhao, H. Cong, P. Li, D. Wu, S. Chen and W. Luo, *Angew. Chem. Int. Ed.*, 2021, DOI: 10.1002/anie.202016207.

17. H. A. Gasteiger, N. Markovic, P. N. Ross and E. J. Cairns, *J. Phys. Chem.*, 1994, **98**, 617-625.

18. H. A. Gasteiger, N. M. Markovic and P. N. Ross, *J. Phys. Chem.*, 1995, **99**, 16757-16767.

19. D. Chen, T. Liu, P. Wang, J. Zhao, C. Zhang, R. Cheng, W. Li, P. Ji, Z. Pu and S. Mu, *ACS Energy Lett.*, 2020, **5**, 2909-2915.

20. J. Zhu, Y. Guo, F. Liu, H. Xu, L. Gong, W. Shi, D. Chen, P. Wang, Y. Yang, C. Zhang, J. Wu, J. Luo and S. Mu, *Angew. Chem. Int. Ed.*, 2021, DOI: 10.1002/anie.202101539.

21. Q. Wu, M. Luo, J. Han, W. Peng, Y. Zhao, D. Chen, M. Peng, J. Liu, F. M. F. de Groot and Y. Tan, *ACS Energy Lett.*, 2020, **5**, 192-199.

22. J. Wang, L. Han, B. Huang, Q. Shao, H. L. Xin and X. Huang, *Nat. Commun.*, 2019, **10**, 5692.

23. S. Liu, X. Mu, W. Li, M. Lv, B. Chen, C. Chen and S. Mu, *Nano Energy*, 2019, **61**, 346-351.

24. Y. Liu, X. Li, Q. Zhang, W. Li, Y. Xie, H. Liu, L. Shang, Z. Liu, Z. Chen, L. Gu, Z. Tang, T. Zhang and S. Lu, *Angew. Chem. Int. Ed.*, 2020, **59**, 1718-1726.

25. J. Yang, B. Chen, X. Liu, W. Liu, Z. Li, J. Dong, W. Chen, W. Yan, T. Yao, X. Duan, Y. Wu and Y. Li, *Angew. Chem. Int. Ed.*, 2018, **57**, 9495-9500.
26. J. Mahmood, F. Li, S.-M. Jung, M. S. Okyay, I. Ahmad, S.-J. Kim, N. Park, H. Y. Jeong and J.-B. Baek, *Nat. Nanotech.*, 2017, **12**, 441-446.
27. Y. Qiao, P. Yuan, C.-W. Pao, Y. Cheng, Z. Pu, Q. Xu, S. Mu and J. Zhang, *Nano Energy*, 2020, **75**, 104881.
28. Z. Pu, I. S. Amiinu, Z. Kou, W. Li and S. Mu, *Angew. Chem. Int. Ed.*, 2017, **56**, 11559-11564.
29. V. Ramalingam, P. Varadhan, H.-C. Fu, H. Kim, D. Zhang, S. Chen, L. Song, D. Ma, Y. Wang, H. N. Alshareef and J.-H. He, *Adv. Mater.*, 2019, **31**, 1903841.
30. Q. Wang, M. Ming, S. Niu, Y. Zhang, G. Fan and J.-S. Hu, *Adv. Energy Mater.*, 2018, **8**, 1801698.
31. J. Zhu, S. Li, M. Xiao, X. Zhao, G. Li, Z. Bai, M. Li, Y. Hu, R. Feng, W. Liu, R. Gao, D. Su, A. Yu and Z. Chen, *Nano Energy*, 2020, **77**, 105212.